THE ASTROPHYSICAL JOURNAL, 461:223–230, 1996 April 10

FORMALDEHYDE ABSORPTION TOWARD SAGITTARIUS A

T. PAULS
Code 7213, Remote Sensing Division, Naval Research Laboratory, Washington, DC 20375-5351
K. J. JOHNSTON
US Naval Observatory, 3450 Massachusetts Avenue, NW, Washington, DC 20392-5420
AND
T. L. WILSON
Max-Planck-Institut für Radioastronomie, Auf dem Hügel 69, D-53121 Bonn, Germany
Received 1995 February 22; accepted 1995 October 24

ABSTRACT

Observations of the 1_{10}–1_{11} line of formaldehyde with an angular resolution of 9.″5 × 20.″6 (P.A. = 4° east of north) toward Sgr A are presented. The velocity resolution is 3 km s^{-1}, and the velocity range extends from −220 to +154 km s^{-1}. The H_2CO line data show that the molecular gas is distributed in clouds ranging in mass from $10^{3.5}$ to $10^{4.8}$ $M_\odot$, with a typical density of $10^{5.5}$ cm^{-3}. These clouds are estimated to be gravitationally stable at present but will have lifetimes of less than 10^6 yr because of tidal forces from Sgr A*. There appears to be an underabundance of formaldehyde in the Galactic center region and particularly in the circumnuclear disk. This may be due to destruction by shocks in this region.

Subject headings: Galaxy: center — ISM: individual (Sagittarius A) — ISM: molecules

1. INTRODUCTION

The radio source Sgr A lies at the dynamical center of the Galaxy (Backer & Sramek 1987; see also the reviews by Genzel & Townes 1987 and Genzel, Hollenbach, & Townes 1994). The region within a few hundred parsecs of Sgr A contains high-density neutral gas, mostly in the form of H_2. Some of this gas seems to move in circular orbits, but there is also significant noncircular motion. The angular resolutions required to study continuum radio features vary from 1′ (2.4 pc; we adopt R_0 = 8 kpc) to milliarcseconds by use of interferometric techniques. For spectral observations, sensitivity limits emission-line observations to resolutions on the order of a few arcseconds, while single-dish data have been measured with beams larger than 8″ (Jackson et al. 1993). Absorption-line measurements are not limited so severely by sensitivity considerations, and these allow the study of gas with low optical depth. Observations of 18 cm OH absorption lines (Sandqvist et al. 1987) and a preliminary H_2CO result (Whiteoak, Gardner, & Pankonin 1983) have been reported.

The 1_{10}–1_{11} K-doublet transition of H_2CO arises from the ground state of orthoformaldehyde. This transition is remarkable in that the excitation temperature T_{ex} is less than 2.7 K for H_2 densities below 10^5 cm^{-3}. This deviation from local thermodynamic equilibrium is believed to be caused by collisions (Townes & Cheung 1969). Thus, this line will absorb the 2.7 K microwave background. For higher values of the H_2 density, the transition will be thermalized and will be seen weakly in emission. There are a very few cases of H_2CO K-doublet emission in our Galaxy. For most of these sources, the excitation is quasi-thermal; a typical example is the emission from the Orion KL Nebula (see, e.g., Johnston et al. 1983). There are a few extremely rare exceptions for which masers are found (Pratap, Menten, & Snyder 1994). In some extragalactic sources, weak maser emission has been found toward the nuclei (Baan, Haschick, & Uglesich 1993).

Observations of H_2CO in the Galactic center region were made with 3′.0 resolution by Bieging et al. (1980). In order to investigate the distribution of H_2CO on a finer angular scale, we have mapped the 10′ area centered on Sgr A* with 9.″5 × 20.″6 resolution to compare absorption-line data with similar maps of OH absorption and molecular emission. Such a comparison of maps of different molecular transitions allows, in principle, a separation of the effects of interstellar chemistry from excitation. From these data, one can obtain information about the density, dynamics, stability, and evolution of the molecular clouds seen toward Sgr A*.

2. OBSERVATIONS

The data were taken on 1988 August 19 with the VLA,[1] using 27 antennas, for a 7 hr synthesis in the D configuration. The observations were made by alternate measurements of the phase calibrator, NRAO 530, and then Sgr A*. For Sgr A*, we used the position R.A. (B1950.0) = $17^h42^m29^s.291$, decl. (B1950.0) = −28°59′17.″6. The source 3C 286 was used as both a bandpass and intensity calibrator. The intensity scale is based on a flux density of 7.46 Jy for 3C 286 at 4.829660 GHz, the line's rest frequency (Lovas 1992). For the spectral line observations, a total bandwidth of 6.25 MHz was used, centered at 40 km s^{-1}, covering, at the line rest frequency, the velocity range from −230 to +150 km s^{-1}, with respect to the local standard of rest. The velocity resolution used was 3 km s^{-1}.

All data calibration and analysis were carried out using the AIPS processing package from NRAO. The continuum levels were set by using the intensities in channels between −70 and −100 km s^{-1} and greater than +135 km s^{-1}. Then the data were placed on 3″ × 3″ grid, using uniform weighting. We used 256 × 256 pixels to cover the 10′ field of

[1] The Very Large Array is operated by the National Radio Astronomy Observatory under a cooperative agreement with the National Science Foundation.

the primary beam. After editing and calibrating the data, we subtracted the continuum emission in the *u-v* plane. The data were then Fourier-transformed and CLEANed. The rms noise in an individual spectral channel was 3.5 mJy beam^{-1}, or 0.9 K main-beam brightness temperature. The beam size was 9″.5 × 20″.6, at P.A. = 4° east of north.

3. RESULTS

3.1. *Continuum Data*

In Figure 1 we show the continuum map produced from the inner 75% of the spectrometer bandpass. Since there is appreciable absorption in the spectral data, we have checked this map against one produced by averaging the channels in which H_2CO absorption is absent. These two maps agree to within the noise. The noise on the continuum map is 0.36 mJy beam^{-1}, or 0.1 K main-beam brightness temperature. The lowest contour in Figure 1 is 56 times the rms noise in the data. The total flux density in our map, integrated over a 3′ × 3′ region, is 69.7 Jy. This is 81% of the flux density measured by use of the Effelsberg 100 m telescope (see, e.g., Bieging et al. 1980).

As with previous maps, our continuum data show the presence of a number of distinct sources. Starting with the largest angular scale, there is a continuum halo over an extent of 5′ (11.7 pc). The location of this region along the line of sight is not certain, but it is most likely close to the Galactic center region. Next is the nonthermal source Sgr A East, which has an FWHP size of 3′ (7 pc). Although not obvious from our data, Sgr A East has a ringlike structure (see the 18 cm continuum map of Sandqvist et al. 1987). Sgr A East may be a supernova remnant, although the energy estimate is ~100 times that of typical Galactic supernova remnants. A more compact source is Sgr A West, with an FWHP size of 2′ (4.7 pc). This source has a spectrum that is consistent with thermal emission. Within the boundaries of this source is the so-called minispiral (with an extent of ~30″), which is only partially resolved in our map. The centers of Sgr A East and Sgr A West are separated, but because the center of Sgr A West is inside the boundary of Sgr A East, its shell structure is, to some extent, filled in.

3.2. *Spectral Line Data*

In Figure 2 we show a series of spectra, obtained by integrating over 15″ × 15″ regions, to orient the reader for the following discussion. Toward the peak of Sgr A* itself, there are a number of fairly narrow absorption features. The velocity components at −55 and 0 km s^{-1} are associated with the "3 kpc arm" and clouds near the Sun, respectively. The deeper absorption centered near +50 km s^{-1}, on the other hand, is associated with the molecular clouds M −0.13 −0.08 and M 0.02 −0.05 (this nomenclature refers to the Galactic coordinates of this region; see Fig. 1 of Güsten, Walmsley, & Pauls 1981). It is believed that both clouds are within a few hundred parsecs of the Galactic center. Comparison of the spectrum toward Sgr A* with spectra toward Sgr A East shows that the −55 and 0 km s^{-1} features are largely unchanged but that the deep absorption has shifted in V_{LSR}. It should also be noted that at large negative radial velocities, in the spectrum taken toward Sgr A* and slightly to its north and east, the base level is slightly below zero, but is exactly zero at other posi-

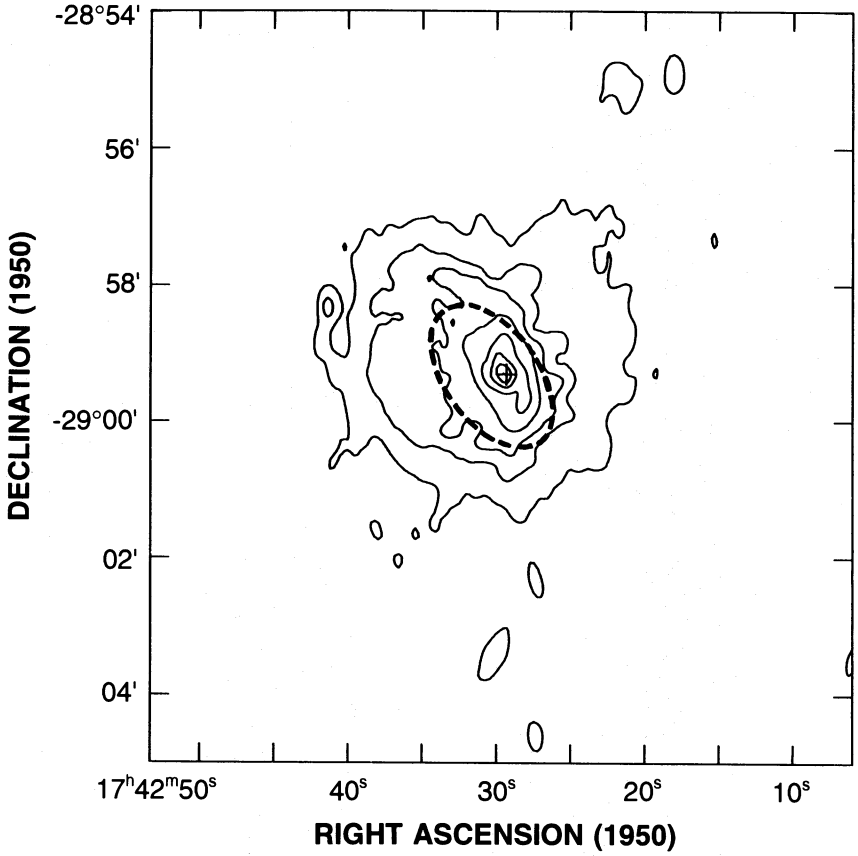

FIG. 1.—Continuum map of the Sgr A region. The cross marks the location of Sgr A*. The dashed ellipse indicates the location and size of the circumnuclear disk. The contour levels are 0.5%, 5%, 10%, 20%, 40%, 60%, and 80% of the peak intensity, 4.07 Jy beam^{-1}. The angular resolution of the map is 9″.5 × 20″.6 at P.A. = 4° east of north.

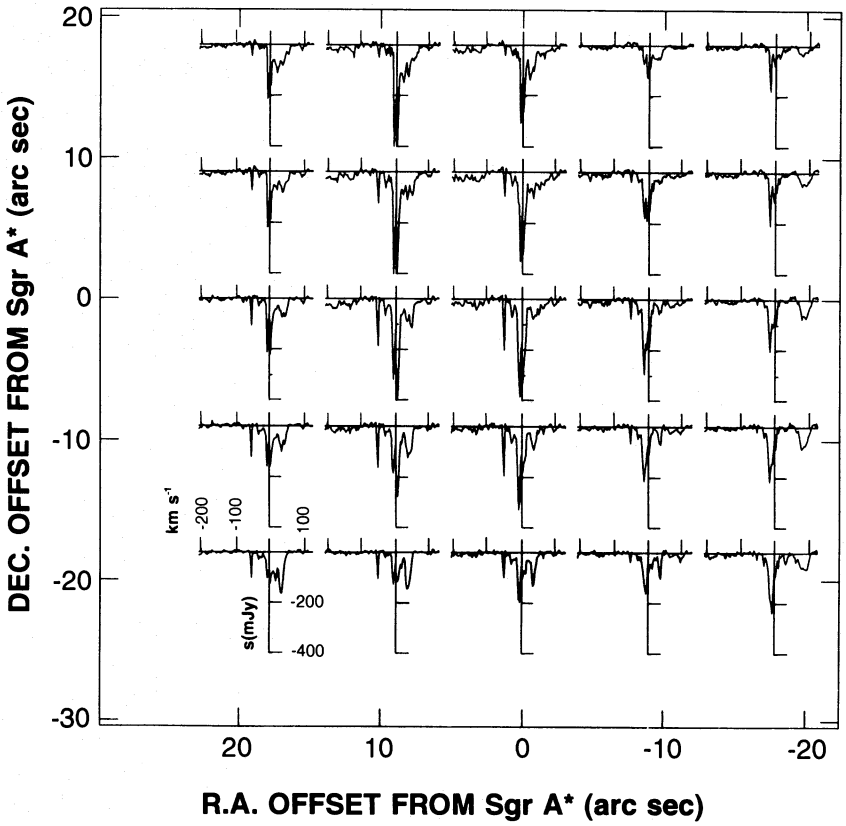

FIG. 2.—Series of H_2CO spectra obtained by integrating 15″ × 15″ regions spaced 9″ apart. The velocity resolution is 3 km s^{-1} and the map center is at R.A. (B1950) = $17^h42^m29^s.291$, decl. (B1950) = −28°29′17″.6.

tions. No baselines have been removed from these spectra. We interpret the negative offset as evidence of weak, broad absorption at negative velocities for directions within 15″ of Sgr A*. This absorption is absent in other nearby directions. In the spectrum 18″ west of Sgr A* there is a molecular cloud with V_{LSR} of about +100 km s^{-1}. Taken together, the very high negative and positive velocity features give support to a picture in which there are large deviations from circular motion close to Sgr A*.

Another version of the data is shown in Figure 3: a longitude-velocity diagram at the latitude of Sgr A*. As can be seen, the gas in the "3 kpc arm" is clearly separated from other features. There is a preponderance of gas at positive velocities, but there is weak absorption extending to −200 km s^{-1}. As dealt with at length in Pauls et al. (1993) for H_2CO and in Marr et al. (1992) for HCO^+, this absorption is close to, but not coincident with, the peak of Sgr A*.

For the molecular gas with V_{LSR} between +100 and −30 km s^{-1} there is a complex pattern of absorption, which will be analyzed next. In this description, we will proceed from positive to negative V_{LSR}. These data will be compared with the $J = 1 \rightarrow 0$ HCN line observations of Güsten et al. (1987), the $J = 3 \rightarrow 2$ HCN line results of Jackson et al. (1993), and the 18 cm OH absorption-line maps of Sandqvist et al. (1987).

Figure 4 displays a series of contour maps of H_2CO absorption in a 3 km s^{-1}–wide channel for radial velocities in the range from −58 to +75 km s^{-1}. The maximum absorption in a single 9″.5 × 20″.6 beam is 1.74 Jy $beam^{-1}$ (−464.3 K), at V_{LSR} = 38.8 km s^{-1}. The lowest contour shown is 15 times the rms noise in a single velocity channel. At this level, there will be absorption only against the brighter continuum features of Sgr A East, Sgr A West, and Sgr A*. Below, we describe the line absorption maps in detail.

At velocities higher than 102 km s^{-1} there is no H_2CO to be seen on the individual channel maps. Between ~75 and 85 km s^{-1}, absorption is found ~10″ west of Sgr A*. This weak feature persists, as a separate entity, to V_{LSR} = 72 km s^{-1}. In contrast, the $J = 3 \rightarrow 2$ line of HCN, integrated over the 90–105 km s^{-1} velocity interval, shows a maximum 40″ northwest of Sgr A*. This peak is also present in a map of the $J = 1 \rightarrow 0$ line of HCN at 129.4 km s^{-1}. In OH absorption, at high positive velocities, there is an elongated streamer in a north-south direction. The total extent is 1′ for V_{LSR} < 80 km s^{-1}. At V_{LSR} = 104 km s^{-1}, the length is 40″.

At 72 km s^{-1}, two additional features appear, one 200″ north and another 100″ to the east of Sgr A*. The feature to the east is close to the position where NH_3 emission was found by Ho et al. (1991). Zylka, Mezger, & Wink (1990) associated this emission with an extension of the +20 an +50 km s^{-1} clouds (M −0.13 −0.08 and M 0.02 −0.05). Both the $J = 3 \rightarrow 2$ and $J = 1 \rightarrow 0$ line HCN data show a peak to the northwest of Sgr A*. The $J = 1 \rightarrow 0$ line maps show a ring of emission extending from west to north to northeast, at 74.4 km s^{-1}. In optical depth, the gas to the east of Sgr A* dominates since the continuum distribution falls off more slowly than the absorption-line intensity.

Between 69.1 and 50.9 km s^{-1}, the H_2CO absorption increases in strength. There is an elongated feature, north-south, centered 100″ east of Sgr A*. At V_{LSR} < 63.1 km s^{-1} there is an absorption feature that extends from Sgr A* to the north by ~20″. At most velocities in this range, this feature is separated from the major absorption. The

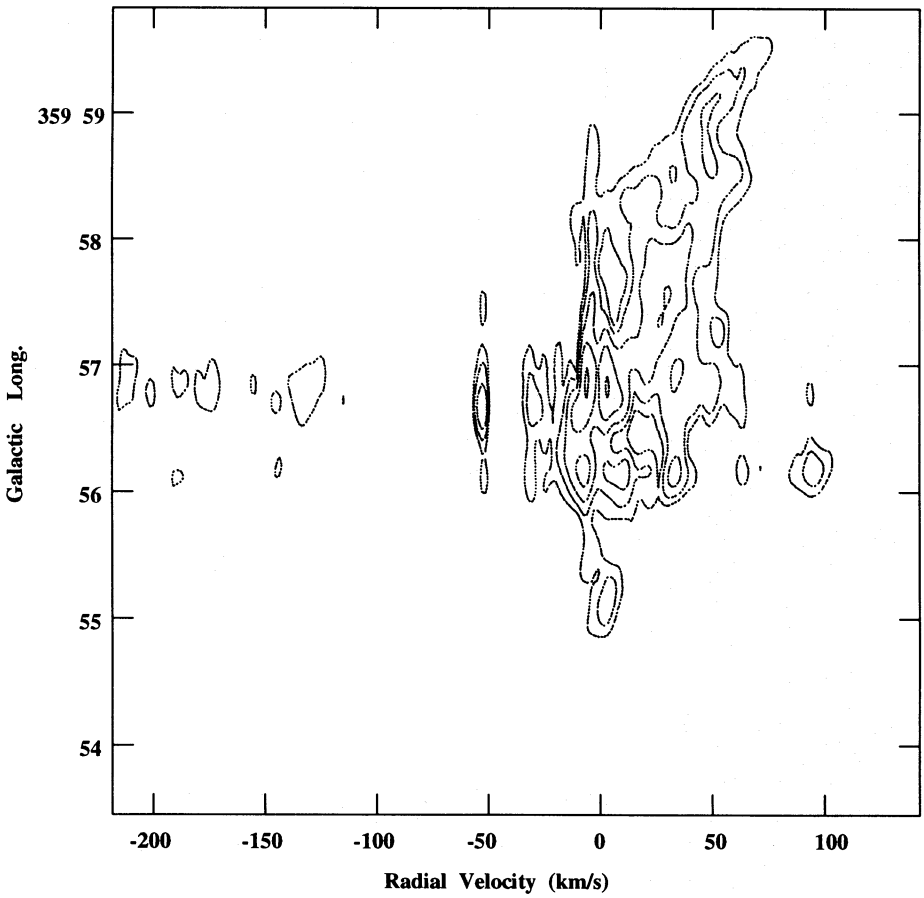

FIG. 3.—Longitude-velocity diagram of the H_2CO absorption at the latitude of Sgr A* (−00°02′45″.2). The contours are −0.400, −0.200, −0.100, −0.050, and −0.025 Jy beam^{-1}. We note that at positive longitudes and velocities there is a general velocity gradient of ∼10 km s^{-1} pc^{-1}.

$J = 1 \rightarrow 0$ HCN lines show different distributions: at 57.5 and 44.8 km s^{-1} there is an arc to the northwest with a peak 20″ northwest of Sgr A*. The $J = 3 \rightarrow 2$ line data are similar, but there is also a weaker peak to the northeast. The OH absorption-line distribution is more similar to that of H_2CO, with a streamer to the west of Sgr A* extending north-south over 1′, which breaks up into two features at lower velocities.

The V_{LSR} range from 47.9 to 11.5 km s^{-1} includes the classical "20 km s^{-1} and 50 km s^{-1} clouds." The absorptions are deep and cover a 2′ × 5′ region in right ascension and declination, centered to the east of Sgr A*. To higher V_{LSR}, there is a continuation to the absorption at ∼70 km s^{-1}. Thus, these results support the idea that there is a connection between gas at 50 km s^{-1} and gas at higher velocities. The absorption at 70 km s^{-1} gives the impression of a more quiescent region. At lower V_{LSR}, the gas shows more rapid changes. At 35.8 km s^{-1} there are absorption peaks south and east of Sgr A*, surrounded by lower intensity, diffuse absorption. The optical depth maxima are ∼50″ east and ∼100″ south of Sgr A*. At 29.7 km s^{-1} the absorption breaks up into two features and has a looplike appearance. The distribution of the OH and H_2CO lines are similar, but there are large differences with the HCN maps. The $J = 1 \rightarrow 0$ line of HCN at 44.8 km s^{-1} shows two features in the west. The first is 1′ and the second is 30″ long; both are oriented north-south. In the $J = 3 \rightarrow 2$ line, there is less detail since there is a spread over a larger velocity range. From 45–60 km s^{-1} to 0–15 km s^{-1}, the maximum shifts from the northwest to the east of Sgr A*.

Between 23.7 and 11.5 km s^{-1}, the absorption covers a region of less than 40″ in right ascension, while the extent in declination is 5′. In right ascension, the absorption is centered on Sgr A* and extends southward. The optical depth is largest for sources between 100″ and 200″ south of Sgr A*. At 11.5 km s^{-1}, this trend continues, with the largest optical depths between 100″ and 300″ south of Sgr A*. The continuum sources located at these southern positions are described in detail by Armstrong & Barrett (1985). There is weak HCN $J = 3 \rightarrow 2$ line emission 14″ east of Sgr A*, elongated north-south over 1′. The OH absorption at 16 km s^{-1} is distributed in the shape of an ellipse, with one side north and south of, but not on, Sgr A*. The other side is 1′ to the east.

The V_{LSR} range from 8.5 to −21.8 km s^{-1} seems to include gas with a wide variety of physical conditions; some gas is near the Sun, and other material is close to the Galactic center. For a V_{LSR} of −0.6 km s^{-1}, the largest optical depths are located at 100″ south and ∼80″ west of Sgr A*. At −3.6 km s^{-1} there is a set of narrow features centered on Sgr A* and to the south. These clouds are probably near the Sun. The absorption in the $J = 1 \rightarrow 0$ line of HCN emission shows similar features; at −15 km s^{-1} there is an arc of emission east of Sgr A*. Emission from the $J = 3 \rightarrow 2$ line of HCN over the 0–15 km s^{-1} interval peaks 20″ southeast and southwest of Sgr A*. The OH absorption at +7 km s^{-1} is found toward Sgr A*; there are also streamers more than 30″ northeast and 30″ north and south of Sgr A*.

In the range −24.8 to −33.9 km s^{-1}, the absorption tends to become less extended with decreasing V_{LSR}. The

1996ApJ...461..223P

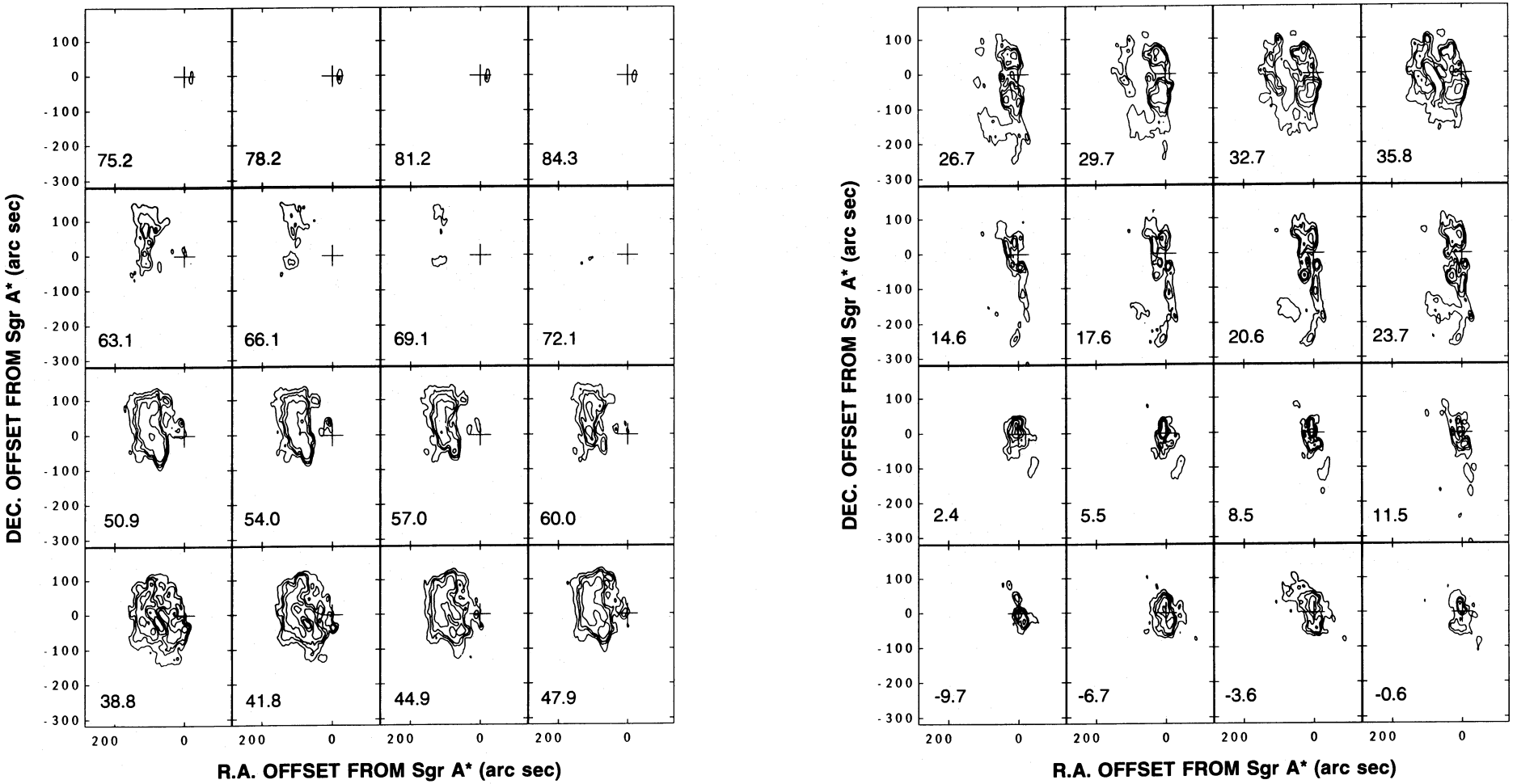

FIG. 4.—Series of contiguous velocity channels showing the absorption in the H_2CO line. The V_{LSR} is given in the lower left corner of each panel. The contour levels are −0.400, −0.200, −0.120, −0.080, and −0.040 Jy beam^{-1}. The lowest absorption-line contour represents 6.67 K brightness temperature, in a 9″.5 × 20″.6 beam. The crosses mark the position of Sgr A*.

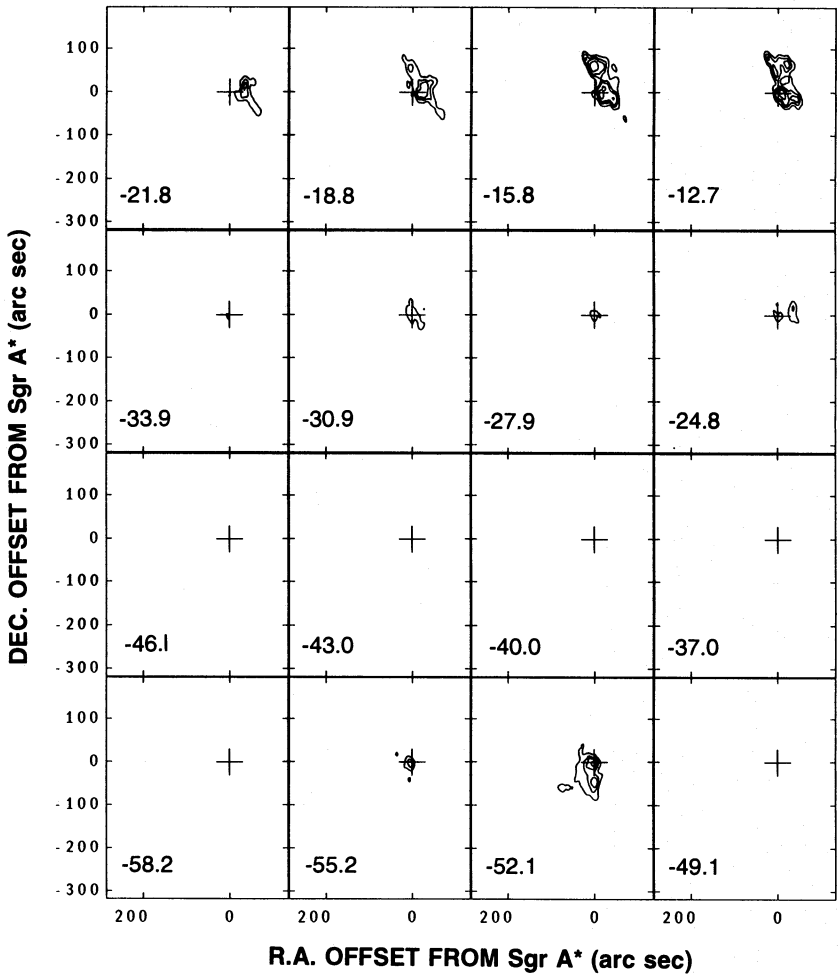

FIG. 4—*Continued*

H_2CO absorption is centered on Sgr A* and is weak. The HCN emission is southeast and southwest of Sgr A*. In the $J = 3 \rightarrow 2$ line, for -30 to -45 km s^{-1}, the total extent is 60″. In the $J = 1 \rightarrow 0$ line, the weak emission at -27.9 km s^{-1} in the southwest extends west for 2′. Presumably, this gas is near Sgr A* itself, because of the rapid change in spatial structure and rather large noncircular velocity.

As mentioned previously, there is narrow absorption at -51.2 and -55.2 km s^{-1} from the "3 kpc arm." Such absorption is also found in OH, centered $\sim 30''$ south of Sgr A*, with a tendency to become stronger in an arclike feature southwest of Sgr A*.

4. ANALYSIS AND DISCUSSION

In this section we extend the largely qualitative discussion of the H_2CO clouds presented above with a quantitative analysis of their sizes, masses, and densities. To this end, we have carried out a Gaussian analysis of the data to determine the cloud sizes in two dimensions, positions, and line widths. We have used only absorption lines with an absolute peak intensity greater than 70 mJy beam^{-1}, that is, 20 times the rms noise. At this level, we find 112 clouds in the Sgr A* region. Since there is high-resolution data for only the 6 cm transition of H_2CO, we cannot carry out a multiline analysis to determine the H_2 column densities or local densities. We therefore calculate these quantities assuming that the clouds seen in H_2CO are in virial equilibrium. From the derived cloud sizes and line widths, we can thus estimate virial masses. Figure 5 shows the distribution of cloud masses (*bottom*) and densities (*top*). In these figures we only include clouds with $|V_{LSR}| \geq 10$ km s^{-1} and exclude the clouds associated with the "3 kpc arm."

Our cloud masses range from 5000 to 40,000 $M_\odot$. From these virial masses and cloud sizes, we have calculated average densities. The H_2 densities show a much smaller spread than cloud masses, with a maximum around $10^{5.5}$ cm^{-3}. These estimates can be very model dependent if influences other than self-gravity are important. Our value for the average density is in good agreement with the estimate of Jackson et al. (1993). Since the H_2 densities of Jackson et al. were not obtained from the virial theorem, the agreement with the densities derived here suggests that these clouds are gravitationally stable. However, an additional cloud-stability criterion involves tidal forces. This criterion (see Stark & Bania 1986; Stark et al. 1989) depends only on the distance from the most massive object, either the central stellar cluster or Sgr A*. The average projected offset is 8 pc, so it appears that, for this density, these clouds are too close to Sgr A*. If they are to be tidally stable, they must be located 4 times farther away than their projected distance. If so, these clouds are distributed in a very asymmetric way, with most clouds at small projected distances. However, there is a strong selection effect in that the sensitivity and the small optical depth of the lines restrict detection of 6

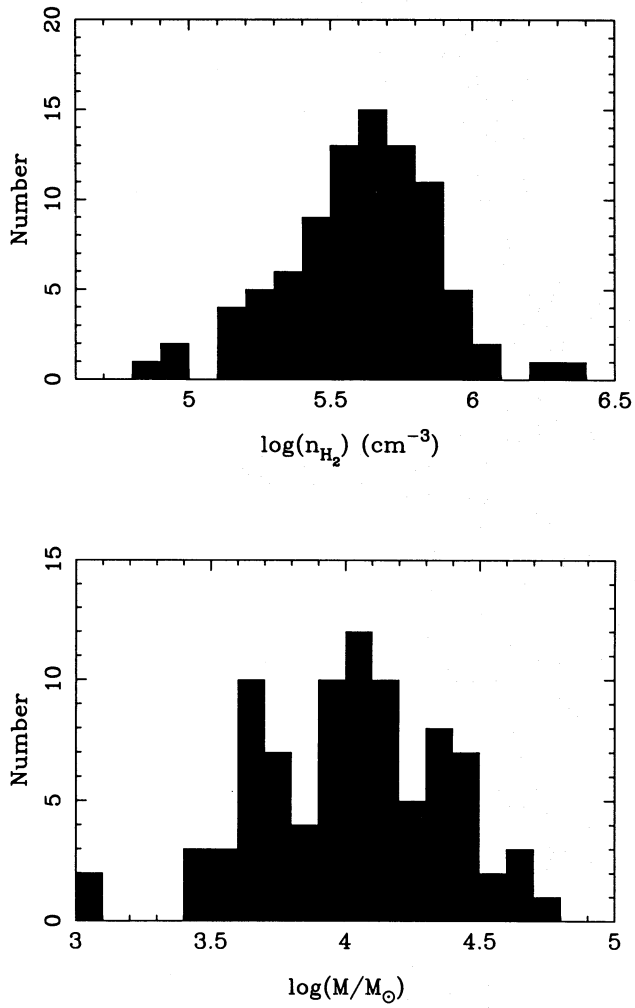

FIG. 5.—Distribution of H_2CO cloud masses (*bottom*) and densities (*top*), obtained by applying the virial theorem to the line widths and sizes obtained from a Gaussian analysis of the data.

cm H_2CO lines to regions in front of continuum sources with main-beam brightness temperatures larger than 1 K. In addition, there is a limit set by the primary beam of the VLA. Thus, on the basis of this analysis, we expect there to be a large number of molecular clouds with radial velocities in the range 20–60 km s^{-1} out to 20′ from Sgr A*.

In addition to cloud stability, there is the question of whether these clouds will be drawn into Sgr A*, as proposed by Ho et al. (1985) and Zylka et al. (1990). Given the radial velocities and angular offsets from Sgr A*, von Linden, Duschl, & Biermann (1993) have concluded that these clouds have too much angular momentum to fall into Sgr A*. Thus, these clouds will supply material for Sgr A* only in very rare cases. Basically, the dynamical situation for these clouds is analogous to that for comets in the solar system. Many comets pass close to the Sun but only very few actually fall into the Sun, because the angular momentum is too large. However, this analogy has another facet: if our density estimates are even approximately correct, and if these clouds pass by Sgr A* at the projected distance, they will break up. Thus, although we conclude that these clouds are virially stable at present, it is likely that they will only have a lifetime of less than 10^6 yr.

The abundance of H_2CO can be determined from an excitation model, taking the H_2 density to be 10^5 cm^{-3}. In order to estimate the 6 cm line optical depths, we have used the measured continuum intensities at the cloud center. We have not corrected for beam dilution, nor have we added in the resolved-out radio continuum flux density. In order to obtain the H_2CO column densities, we have assumed that T_{ex} is 2.7 K to calculate the column density in the 1_{11} level. We then doubled this value to obtain the column density in the 1_{11} level and then assumed that this was the total column density in ortho-H_2CO. This neglects populations in the higher rotational levels, but should be accurate to $\sim$30%. To account for the population of para-H_2CO, we then multiplied this value, for each cloud, by 1.3. We find an average relative abundance of order 5×10^{-10}, which is 5% of the usual result for dark clouds near the Sun (see Irvine et al. 1985).

Compared to the abundance of other molecules close to Sgr A*, from the distribution of V_{LSR} and positions it is clear that we find little H_2CO in the circumnuclear disk (CND). This might be caused by a combination of sensitivity and excitation effects, if the excitation temperature of the 6 cm transition is close to the brightness temperature of the background continuum. From the H_2 densities, this last suggestion seems unlikely. In order to check further, we have carried out limited measurements of the 2_{12}–1_{11} rotational transition, at 2 mm wavelength, with the IRAM 30 m telescope. (More complete data, with 1′ resolution, are presented by Sandqvist 1989.) Our data were taken with beam switching, using a 4′ beam throw, to avoid instrumental baseline effects. These data confirm the 6 cm line results. There is an indication of weak H_2CO emission from the CND at 2 mm wavelength. These results yield a column density of at most 10^{12} cm^{-3}. Thus, there must be a substantial deficiency of H_2CO in the CND. The 18 cm OH data of Sandqvist et al. (1987) show that although OH is present in the CND, the absorption is rather weak, even though the background continuum intensity is larger. Since OH is usually more abundant than H_2CO, this result should be taken as a confirmation that H_2CO and OH are underabundant in the CND. This may be related to the large line widths observed to be present in the CND. These line widths are due to turbulence in the CND and may be an indication of shock waves in the CND, which is physically close to Sgr A*. We hypothesize that fragile molecules such as H_2CO and OH may be destroyed by shock waves in the CND.

Here we have only analyzed molecular gas with V_{LSR} between -60 and $+70$ km s^{-1}. The high negative and positive velocity material discussed by Pauls et al. (1993) has not been included because the intensity is below the cutoff used for the fitting procedure. For this material, the most interesting question is whether the clouds are close to Sgr A* or more than 100 pc from this source. Liszt & Burton (1993) and Yusef-Zadeh, Lazenby, & Marshall (1993) have addressed this question and come to opposite conclusions.

We have estimated the H_2 density of the gas that is moving between -160 and -200 km s^{-1} by observing the $J = 2 \rightarrow 1$ and $J = 1 \rightarrow 0$ lines of CO with the IRAM 30 m telescope. In order to obtain an average over the entire cloud seen in H_2CO, we averaged the CO data over a 20″ × 20″ region, using uniform weighting, centered on the high negative velocity H_2CO feature. The $J = 2 \rightarrow 1$ line data show a peak main-beam temperature that is $\sim$0.6 times that found in the $J = 1 \rightarrow 0$ line. Using a large velocity gradient model yields a density of $\sim$700 cm^{-3}, for a

kinetic temperature of 100 K. Given this low H_2 density, this cloud will not be tidally stable if it is within 500 pc of Sgr A. Thus, either the high negative velocity gas is stable and more than 500 pc from Sgr A, or it is near Sgr A and destined to break up.

5. CONCLUSIONS

On the basis of our 6 cm line maps of H_2CO made with the VLA, and additional data taken with the IRAM 30 m telescope, we conclude as follows:

1. The H_2CO in the streamer at $+50$ to $+70$ km s^{-1} to the east of Sgr A* has an H_2 density of $\sim 10^{5.5}$ cm^{-3} if the clouds are in virial equilibrium.

2. This gas must be at more than 4 times the projected distance in order to be tidally stable. According to the analysis of von Linden et al. (1993), this material will not fall into Sgr A*.

3. The relative abundance of H_2CO is 5×10^{-10}. This is $\sim 5\%$ of the abundance found for dust clouds in the solar neighborhood. There is an even larger underabundance of H_2CO in the circumnuclear disk. Presumably, shock waves dissociate this rather fragile molecule.

4. The streamer gas is further from Sgr A* than the CND. The -200 km s^{-1} gas must be even further, but it is not clear how to bring such material to the very large negative velocities observed.

We wish to thank Angela Linhardt for assistance with data reduction and Gaussian analysis and G. Dahmen for help with the CO observations.

REFERENCES

Armstrong, J. T., & Barrett, A. H. 1985, ApJS, 57, 535
Baan, W. A., Haschick, A. D., & Uglesich, R. 1993, ApJ, 415, 140
Backer, D. C., & Sramek, R. A. 1987, in AIP Conf. Proc. 155, The Galactic Center, ed. D. C. Backer (New York: AIP), 163
Bieging, J., Downes, D., Wilson, T. L., Martin, A. H. M. M., & Güsten, R. 1980, A&AS, 42, 163
Genzel, R., Hollenbach, D., & Townes, C. H. 1994, Rep. Prog. Phys., 57, 417
Genzel, R., & Townes, C. H. 1987, ARA&A, 25, 377
Güsten, R., Genzel, R., Wright, M. C. H., Jaffe, D. T., Stutzki, J., & Harris, A. I. 1987, ApJ, 318, 124
Güsten, R., Walmsley, C. M., & Pauls, T. 1981, A&A, 103, 197
Ho, P. T. P., Ho, L. C., Szczepanski, J. C., Jackson, J. M., Armstrong, J. T., & Barrett, A. H. 1991, Nature, 350, 309
Ho, P. T. P., Jackson, J. M., Barrett, A. H., & Armstrong, J. T. 1985, ApJ, 288, 575
Irvine, W. M., Schloerb, F. P., Hjalmarson, A., & Herbst, E. 1985, in Protostars and Planets II, ed. D. C. Black & M. S. Matthews (Tucson: Univ. Arizona Press), 579
Jackson, J. M., Geis, N., Genzel, R., Harris, A. I., Madden, S., Poglitsch, A., Stacey, G. J., & Townes, C. H. 1993, ApJ, 402, 173
Johnston, K. J., Palmer, P., Bieging, J. H., & Wilson, T. L. 1983, ApJ, 271, L89
Liszt, H., & Burton, B. 1993, ApJ, 407, L25
Lovas, F. J. 1992, J. Phys. Chem. Ref. Data, 21, 181
Marr, J. M., Rudolph, A., Pauls, T. A., Wright, M. C. H., Backer, D. C., & Tucker, L. M. 1992, ApJ, 400, L29
Pauls, T., Johnston, K. J., Wilson, T. L., Marr, J. M., & Rudolph, A. 1993, ApJ, 403, L13
Pratap, P., Menten, K. M., & Snyder, L. E. 1994, ApJ, 430, L129
Sandqvist, A. 1989, A&A, 223, 293
Sandqvist, A., Karlsson, R., Whiteoak, J. B., & Gardner, F. F. 1987, in AIP Conf. Proc. 155, The Galactic Center, ed. D. C. Backer (New York: AIP), 95
Stark, A. A., Bally, J., Wilson, R. W., & Pound, M. W. 1989, in IAU Symp. 136, The Center of the Galaxy, ed. M. Morris (Dordrecht: Kluwer), 129
Stark, A. A., & Bania, T. M. 1986, ApJ, 306, L17
Townes, C. H., & Cheung, A. C. 1969, ApJ, 157, L103
von Linden, S., Duschl, W., & Biermann, P. L. 1993, A&A, 269, 169
Whiteoak, J. B., Gardner, F. F., & Pankonin, V. 1983, MNRAS, 202, 11P
Yusef-Zadeh, F., Lazenby, A., & Marshall, J. 1993, ApJ, 410, L27
Zylka, R., Mezger, P. G., & Wink, J. E. 1990, A&A, 234, 133